Equilibrium properties of the fluxoid lattice in single-crystal niobium. I. Magnetization measurements

H. R. Kerchner, D. K. Christen, and S. T. Sekula
Solid State Division, Oak Ridge National Laboratory, Oak Ridge, Tennessee 37830
(Received 30 April 1979)

The field derivative of the superconducting magnetization (dM/dH_a) of a single-crystal niobium sphere was measured with the applied magnetic field parallel to the three high-symmetry crystal axes. A field-sweep technique was used to make direct, continuous measurements of dM/dH_a, and the data were numerically integrated to obtain the magnetization M. Excellent magnetic reversibility indicates the attainment of equilibrium conditions. The Meissner state, the intermediate mixed state, the mixed state, and the normal state show up as distinct field regions of the dM/dH_a vs H_a plots separated by discontinuities in dM/dH_a. The results are compared with microscopic theory and with related experimental studies of niobium. The magnetization measurements are compared directly with small-angle neutron-diffraction measurements of the fluxoid lattice in the same sample reported in the following paper.

I. INTRODUCTION

A. Motivations for this work

In this paper and the following one[1] (hereafter referred to as II), we describe a thorough study of the equilibrium mixed state of a niobium crystal by magnetization and small-angle neutron-diffraction measurements. By combining the two types of measurements on one sample, we have been able to make direct comparisons between observations of the microscopic structure of the fluxoid lattice and the macroscopic flux density. The neutron-diffraction technique proved to be most useful for measuring the fluxoid lattice symmetry and the flux density precisely at low fields, while the bulk magnetization measurements enabled (less precise) investigation over the whole field range up to the upper critical field.

The equilibrium magnetization of niobium has been investigated experimentally by a number of workers[2–11] and has served as a test of the Ginzburg-Landau-Abrikosov theory of the mixed state and its extensions.[12] In addition, the anisotropy of the upper critical field in single-crystal niobium has been carefully studied.[5–6,13–18] We extend this work by measuring the anisotropy of the magnetization throughout the mixed state. Moreover, since we have measured the field derivative of the magnetization directly, our results for this quantity may be compared with theoretical values at the upper critical field more reliably than is possible with earlier measurements. Our technique also makes available for the first time an experimental determination of the field derivative of the magnetization at the lower critical field. In addition, the excellent reversibility of our samples makes our determination of the lower critical field more reliable than earlier measurements.

Although most of the isotropic microscopic theory of the mixed state has been compared adequately with the measurements on polycrystalline niobium, some recent theoretical advances have not been compared in the literature. Therefore, this paper includes a brief review of the relevant theoretical results and their comparison with our experimental values averaged over all crystal orientations. In addition, we present direct comparisons between our data and the most comparable previous data where our measurements repeat earlier ones.

There has been a theoretical and experimental effort to understand the relative anisotropy of the upper critical field of niobium. Although no theory at present exists for the anisotropy of the magnetization, some calculations are in progress.[19] It is hoped that our measurements will stimulate further theoretical effort in this area.

B. Thermodynamics of the mixed state

In order to better present the salient features of the magnetization data, we first review the thermodynamic description of the equilibrium mixed state. Equilibrium in the mixed state occurs at the minimum of the Gibbs potential

$$g = f(\vec{B}) - \frac{1}{4\pi}\vec{B}\cdot\vec{H} \ , \tag{1}$$

where $\vec{B}$ is the macroscopic flux density, $f(\vec{B})$ is the Helmholtz free-energy density of the material, and $\vec{H}$ is the equilibrium magnetic field defined thermodynamically by

$$\vec{H} = 4\pi\nabla_{\vec{B}} f \ , \tag{2}$$

where $\nabla_{\vec{B}}$ is the gradient with respect to $\vec{B}$. The free-energy density $f(\vec{B})$ must be calculated by using microscopic theory with some material-dependent parameters. In an isotropic material, f does not depend on the direction of $\vec{B}$, but only its magnitude. In general, f depends on the orientation of $\vec{B}$ with respect to the crystal, and $\vec{H}$ and $\vec{B}$ may have different directions. In practice, f depends only weakly on the direction of $\vec{B}$, so that the angle between $\vec{B}$ and $\vec{H}$ is small.

In niobium and other type-II superconductors with low Ginzburg-Landau parameter κ (see Sec. I E), $|\nabla_{\vec{B}} f|$ initially decreases as B is increased from zero, goes through a minimum, and then increases with B at larger B. The presence of the minimum of $|\nabla_{\vec{B}} f|$ produces a first-order transition between the Meissner state ($\vec{B}=0$) and the mixed state. At this transition the fluxoid lattice of flux density $\vec{B}_0$ is in equilibrium with the Meissner state and with the magnetic field $\vec{H}_{c1}$. That is,

$$\vec{H}_{c1}=4\pi\nabla_{\vec{B}} f|_{\vec{B}_0} \tag{3}$$

and

$$g=f(\vec{B}_0)-\frac{1}{4\pi}\vec{B}_0\cdot\vec{H}_{c1}=f(0)\ . \tag{4}$$

In materials with higher κ, $|\nabla_{\vec{B}} f|$ increases monotonically with B, the transition is second order, and $\vec{H}_{c1}$ is given by

$$\vec{H}_{c1}=4\pi\lim_{B\to 0}\nabla_{\vec{B}} f\ . \tag{5}$$

Microscopically, when the transition is second order, the interaction between fluxoids is always repulsive. A first-order transition is associated with a long-range attractive interaction between fluxoids that produces the minimum in $|\nabla_{\vec{B}} f|$. At the field $\vec{H}_{c1}$, fluxoids in a low-κ type-II superconductor are separated by the equilibrium spacing associated with the flux density B_0. At flux densities B larger than B_0, the fluxoids repel each other and are in equilibrium with a larger field $\vec{H}$.

The Gibbs potential of the mixed state is lower than the Gibbs potential of the normal state ($\vec{B}=\vec{H}$) for all values of $\vec{B}$ below the upper critical field $\vec{H}_{c2}$. At $\vec{H}_{c2}$, the mixed state and normal state are in equilibrium, and their Gibbs potentials are equal. Integrating Eq. (2) over any equilibrium path and using the equilibrium condition at H_{c2}, one readily arrives at the conclusion that the condensation energy of the superconducting state is given by

$$f(0)-f_n(0)=\frac{1}{4\pi}\int_0^{\vec{H}_{c2}}(\vec{B}-\vec{H})\cdot d\vec{H}\ , \tag{6}$$

where $f_n(0)$ is the free-energy density of the normal state in zero field. The thermodynamic critical field H_c is defined by

$$\frac{1}{8\pi}H_c^2=f(0)-f_n(0)\ . \tag{7}$$

Unlike $\vec{H}_{c1}$ and $\vec{H}_{c2}$, H_c is independent of the direction of $\vec{B}$.

The occurrence of a first-order phase transition at $\vec{H}_{c1}$ suggests the possibility of metastable states.[20] The Meissner state may persist (superheat) in increasing field above H_{c1} until the field in equilibrium with an isolated fluxoid

$$\vec{H}_{c1}^{*}=4\pi\lim_{B\to 0}\nabla_{\vec{B}} f\ , \tag{8}$$

is reached. When the transition is first order, $H_{c1}^{*}>H_{c1}$. In an ideal sample initially in the Meissner state, isolated fluxoids must be created at the surface before they can fall in to form the lattice of flux density $\vec{B}_0$. Thus when flux first enters the sample the field must be at least H_{c1}^{*}. However, if the sample is not ideal, any defect at the surface that permits the formation of fluxoid lattice (e.g., a region with a low H_{c1}) serves as a nucleation site for the mixed state as long as the field is larger then H_{c1}.

Likewise, the mixed state may supercool in decreasing field to the minimum value of $4\pi|\nabla_{\vec{B}} f|$ $<H_{c1}$. The minimum supercooling field may not be observed because some defect in the sample may permit nucleation of the Meissner state at a larger field. Since we always observe a nonzero $\nabla_{\vec{B}}\cdot\vec{H}=4\pi\nabla_{\vec{B}}^2 f$, we conclude that we have never supercooled the mixed state to the minimum of $4\pi|\nabla_{\vec{B}} f|$. Evidence for some slight supercooling of the mixed state will be presented in the accompanying paper.

Metastable states can also occur as a result of fluxoid pinning by microscopic defects in the sample[21] and as a result of the interaction of fluxoids with the shielding currents at the surface of the sample.[22] The sample was prepared in such a way to minimize both these effects. The sample preparation is described below.

C. Magnetization of a sphere

Because the presence of a magnetic sample distorts the magnetic field, the relation between the applied field (as measured by the external current producing it) and the induced moment or the flux density is not direct. However, the boundary conditions are such that a uniform applied magnetic field produces a uniform magnetization in a homogeneous ellipsoidal sample. Moreover, the applied field $\vec{H}_a$ is related in a simple way to the magnetization $\vec{M}$, the flux density $\vec{B}$, and the field $\vec{H}$ that is in equilibrium with $\vec{B}$. The shape of the ellipsoidal sample is described by a demagnetization tensor $\underline{D}$. The relation is

$$\vec{H}=\vec{H}_a-4\pi\vec{M}\cdot\underline{D}\ ,$$

where the magnetization as usual is

$$\vec{M}=\frac{1}{4\pi}(\vec{B}-\vec{H})\ . \tag{9}$$

For a sphere, $\underline{D}$ is a scalar equal to one third, and

$$\vec{H} = \vec{H}_a - \tfrac{4}{3}\pi\vec{M} \ . \tag{10}$$

The applied field $\vec{H}_a$ is identical to the field in the absence of the sample, and it can be measured independently of the magnetization of the sample by measuring the current that generates it. The magnetic field $\vec{H}$ outside the sample is the sum of $\vec{H}_a$ and the nonuniform field produced by the moment of the sample. The field produced by a uniformly magnetized sphere is a dipole field.

In general, $\vec{B}$ depends on the orientation of the sample in the applied field $\vec{H}_a$ and is not parallel to $\vec{H}_a$ even for an isotropic material. In order to observe small anisotropies of material parameters, it is necessary to know the sample geometry accurately. The best way of accomplishing this end is to use a spherical sample, because $\underline{D}$ is a scalar for a sphere and because it is possible to make a sample accurately spherical.

A type-II superconductor with a first-order transition at $\vec{H}_{c1}$ (hereafter referred to as type-II/1) exhibits an intermediate mixed state (IMS) that is analogous to the intermediate state of a type-I superconductor. In a sphere, the Meissner state is stable only for applied fields less than $\frac{2}{3}\vec{H}_{c1}$. As $\vec{H}_a$ is raised above $\vec{H}_1 = \frac{2}{3}\vec{H}_{c1}$, mixed-state domains of flux density $\vec{B}_0$, which are in equilibrium with the Meissner-state domains, gradually fill the sample. Setting $\vec{H} = \vec{H}_{c1}$ in Eq. (10), we see that the magnetization increases linearly from the value $-\vec{H}_{c1}/4\pi$ at $\vec{H}_a = \frac{2}{3}\vec{H}_{c1}$ to the value $-(\vec{H}_{c1} - \vec{B}_0)/4\pi$ at $\vec{H}_a = \vec{H}_2 = \frac{2}{3}\vec{H}_{c1} + \frac{1}{3}\vec{B}_0$, where the sample is filled with fluxoid lattice. As the field is further increased, the fluxoids move closer together until the magnetization disappears at the upper critical field H_{c2}.

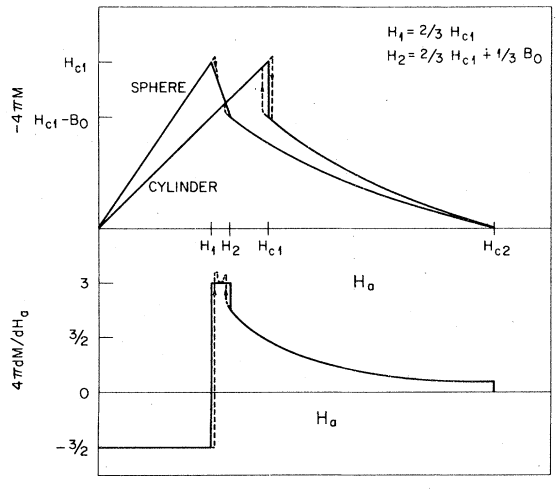

FIG. 1. Ideal magnetization curves $M(H_a)$ of a long cylinder in an axial field and a sphere of the same material, and dM/dH_a of the sphere. The solid curves indicate the equilibrium magnetization, while the dashed curves illustrate superheating and supercooling effects.

The magnetization curve of a spherical type-II/1 superconductor and its derivative are illustrated schematically in Fig. 1 and compared with the magnetization curve of an infinite cylinder of the same (isotropic) material in the axial field. In the Meissner state ($H_a < \frac{2}{3}H_{c1}$) and in the intermediate mixed state ($\frac{2}{3}H_{c1} < H_a < \frac{2}{3}H_{c1} + \frac{1}{3}B_0$), the equilibrium magnetization plot depends only on the shape of the sample and on H_{c1}. In the mixed state, the repulsive interaction between fluxoids produces the curvature shown. The field derivative of the magnetization is discontinuous at each of the three transitions—between the Meissner state and the IMS, between the IMS and the mixed state, and between the mixed state and the normal state. Because of the discontinuities, a direct measurement of dM/dH_a is most useful for identifying the transition fields. The solid curves in Fig. 1 represent the equilibrium situation. The effects of superheating the Meissner state and supercooling the mixed state are indicated by dashed curves.

D. Misalignment between $\vec{B}$ and $\vec{H}$

The flux density $\vec{B}$, and field $\vec{H}$, and the magnetization $\vec{M}$ are not parallel in general. However, the symmetry of the free energy $f(\vec{B})$ (as well as every other scalar function of a vector argument) must reflect the symmetry of the crystal. As a result, the free energy as a function of the direction of $\vec{B}$ must have extrema at the high-symmetry crystal directions, and $\vec{H}$ must be parallel to $\vec{B}$ at those directions. At off-symmetry directions $\vec{B}$ and $\vec{H}$ are not parallel by virtue of the fact that f depends on the direction of $\vec{B}$. The mathematical statement of these characteristics is

$$|\vec{B}\times\vec{H}| = 4\pi|\vec{B}\times\nabla_{\vec{B}}f| = 4\pi|\nabla_{\hat{B}}f| > 0 \tag{11}$$

except at the extrema of $f(\hat{B})$. Here $\hat{B}$ is the unit vector in the direction of $\vec{B}$ and $\nabla_{\hat{B}}$ is the two-dimensional gradient on the surface of the unit spheres in $\vec{B}$ space.

Associated with a misalignment between $\vec{B}$ and $\vec{H}$ is a torque $\vec{\tau}$ on the sample,

$$\vec{\tau} = \int_{s+s'} \hat{H}_a \times \nabla_{\hat{H}_a} g \, dV = \int_s \vec{M}\times\vec{H}_a \, dV \ , \tag{12}$$

where $\nabla_{\hat{H}_a}$ is the two-dimensional gradient on the surface of the unit sphere in $\vec{H}_a$ space. The volume s

is the volume of the sample, and $s+s'$ is all space. Equation (12) follows from the well-known relation

$$\int_{s+s'} dg\, dV = \int_s \vec{M}\cdot d\vec{H}_a\, dV - \frac{1}{8\pi}\int_{s+s'} d(H_a^2)\, dV \quad . \tag{13}$$

The torque on a niobium crystal in the mixed state has been measured by Holzhäuser[23] and by Schneider *et al.*[24] The neutron-diffraction measurements described in II are the first direct observation of the misalignment.

Although the relation between the misalignment angle and the anisotropy of the magnetization is rather complicated in general, two simple relations can be derived at $\vec{H}_{c1}$ and $\vec{H}_{c2}$. Near $\vec{H}_{c2}$ both the torque and the magnetization go to zero in proportion to $H_{c2}-H$, but the angle ϵ between $\vec{M}$ and $\vec{H}$ approaches a finite value. The angle ϵ is given by

$$\begin{aligned}\tan\epsilon(\vec{B}) &= |\vec{M}\times\vec{H}|/|\vec{M}\cdot\vec{H}| \\ &= |\vec{B}\times\vec{H}|/|\vec{B}\cdot\vec{H}-H^2| \\ &= |\nabla_{\hat{B}}f|/\left|B\frac{\partial f}{\partial B}-4\pi\left(\frac{\partial f}{\partial B}\right)^2-4\pi\left(\frac{\nabla_{\hat{B}}f}{B}\right)^2\right| \quad .\end{aligned} \tag{14}$$

Expanding both the numerator and the denominator to first order as a Taylor series in $(B-H_{c2})$, we obtain

$$\tan\epsilon(\vec{B}) = \frac{4\pi|(\partial/\partial B)(\nabla_{\hat{B}}f)+\cdots|}{H_{c2}[1-4\pi(\partial^2 f/\partial B^2)|_{\vec{H}_{c2}}]+\cdots} \quad . \tag{15}$$

Differentiating the relation $H_{c2}(\hat{B}) = 4\pi(\partial f/\partial B)|_{\vec{H}_{c2}}$ leads to

$$\nabla_{\hat{B}}H_{c2} = \frac{4\pi(\partial/\partial B)(\nabla_{\hat{B}}f)}{1-4\pi(\partial^2 f/\partial B^2)|_{\vec{H}_{c2}}} \quad . \tag{16}$$

Then

$$\tan\epsilon(\vec{H}_{c2}) = |\nabla_{\hat{B}}H_{c2}|/H_{c2} \quad . \tag{17}$$

A similar argument is used in II to relate the angle between $\vec{B}_0$ and $\vec{H}_a$ in the IMS to the anisotropy of H_{c1}.

E. Microscopic theory of the mixed state

The microscopic theory of the mixed state has been reviewed thoroughly by Fetter and Hohenberg.[12] In what follows we review briefly those theoretical results that can reasonably be compared with our data. We discuss some recent results that have appeared since Ref. 12.

The first theory of the mixed state was developed by Abrikosov[25] on the basis of the phenomenological Ginzburg-Landau theory.[26] All later theories depend heavily on the concepts introduced by Abrikosov. The Ginzburg-Landau theory was assumed to describe superconductors with spatially varying properties near the critical temperature T_c. Abrikosov showed that a mixed state should exist when the material parameter κ was larger than $2^{-1/2}$, and he calculated the upper critical field H_{c2}, the field derivative of the magnetization at H_{c2}, and the lower critical field H_{c1}. To the extent that Ginzburg-Landau theory applies to any real material, extrapolation of measured values of H_{c1}/H_c, H_{c2}/H_c, and $[dM/dH]_{H_{c2}}$ to T_c should be given by the single parameter κ.

Shortly after the introduction of the microscopic theory of superconductivity by Bardeen, Cooper, and Schrieffer (BCS),[27] Gor'kov extended the BCS theory to permit calculations of spatially varying properties.[28] He showed that the Ginzburg-Landau equations followed from the microscopic theory when $T_c - T \ll T_c$. At lower temperatures, the Gor'kov equations include nonlocal effects; therefore, they have a more complicated form than the Ginzburg-Landau equations. Gor'kov's theory has permitted the generalization of Abrikosov's theory to all temperatures. It also provides a basis for understanding the influence on mixed-state properties of electron scattering by impurities.

Historically, the first solution of Gor'kov's equations at lower temperatures was in the limit of short electron mean free path (dirty limit).[29] However, those theoretical results cannot be applied to our relatively clean sample. The first extensions of the Abrikosov theory to pure materials at lower temperatures were the calculation of the temperature dependence of H_{c2} by Helfand and Werthamer,[30] and the calculations of the limiting temperature dependence of H_{c1}/H_c, H_{c2}/H_c, and $[dM/dH]_{H_{c2}}$ at T_c by Neumann and Tewordt.[31] Later, Eilenberger calculated H_{c2}/H_c and $[dM/dH]_{H_{c2}}$ at arbitrary temperatures.[32] Eilenberger's solution gave the wrong value of $[dM/dH]_{H_{c2}}$. The problem was first noted by U. Brandt[33] and later discussed in more detail by Delrieu[34] and E. H. Brandt.[35] Pesch and Kramer solved Gor'kov's equations for an isolated fluxoid, thus determining H_{c1}^*, at arbitrary temperatures and mean free paths.[36] Recently, E. H. Brandt has given numerical solutions of the Gor'kov equations for pure materials at all temperatures and fields.[37] (In Ref. 37 Brandt also reviews recent developments in Gor'kov theory.)

The microscopic theroy of BCS and Gor'kov is based on the free-electron model of a metal with a vanishingly small electron-phonon interaction. Certain band-structure and many-body effects can be incorporated into the microscopic theory simply by renormalizing the free-electron-model parameters. However, certain other real-metal effects such as multiple bands, a finite retarded electron-phonon in-

teraction, and anisotropy of the Fermi surface and of the electron-phonon interaction cannot be incorporated into the theory in a simple way. As a result, BCS theory predicts several universal laws of corresponding states that are only approximately obeyed by real materials. Similarly, the temperature dependences of observable quantities predicted by BCS theory (and by Gor'kov theory) differ from the observed dependences, and anisotropy cannot be described theoretically. The application of completely realistic microscopic theory to some of our data will be discussed elsewhere. Here we consider the influence of Fermi-surface anisotropy on the mixed state. Hohenberg and Werthamer[38] calculated the relative anisotropy of H_{c2} in the nearly local limit (applicable near T_c) and showed that anisotropy can enhance $H_{c2}(T)/T_c[(dH_{c2}/dT)|_{T_c}]$. Recently, Teichler has related the relative anisotropy of H_{c2} at all temperatures to the anisotropy of the Fermi surface and of the electron-phonon coupling for cubic superconductors with arbitrary mean free path.[39] Takanaka and Hubert[40] have calculated H_{c1}^*, and Takanaka and Nagashima[41] and more recently Berthel and Pietrass[42] have given $(dM/dH)|_{H_{c2}}$ in the nearly local limit, for a material with an anisotropic Fermi surface.

A recent theoretical development has been the use of field theoretical techniques to derive equations for the spatial variation of magnetic fields in superconductors. Like Gor'kov's theory, the new approach is based on the BCS model Hamiltonian; however, the solution involves a different set of approximations. The result, which has been named the boson formalism,[43] is a set of field equations that are analogous to, but simpler than, Gor'kov's equations. The theory is incomplete in that the energy associated with the normal core of the fluxoid is taken into account in a phenomenological way and is not a fundamental part of the solution. Also, it is unclear at the present time whether the boson theory reduces to Ginzburg-Landau theory near T_c.

In the boson formalism the parameter κ_B plays a role similar to that of κ in Gor'kov theory. The boson-theory parameter κ_B may be calculated within Gor'kov theory to be $\kappa_B = 1.04\kappa$. Although a unique value of κ for niobium may be determined by extrapolating features of the magnetization curve to T_c, the value of κ_B obtained by multiplying the experimentally determined κ by 1.04 suffers from the deficiencies of Gor'kov theory mentioned above. Therefore, that value of κ_B may not be appropriate for comparing boson-theory results with data. The phenomenological parameter $\delta = H_{c2}(0)/H_c(0)$ enters the theory independently of κ_B. In the boson formalism, the finite electron-phonon interaction is described in an approximate way by a single parameter $N(0)V$. Mixed-state properties appear to be weakly dependent on $N(0)V$. Calculations are in progress to determine the effects of anisotropy of the Fermi surface and of the electron-phonon interaction.[19]

In comparing the results of Gor'kov theory with our data, we have made use of the experimental value of κ obtained by extrapolating our measurements of H_{c2}/H_c and $(dM/dH)|_{H_{c2}}$ to T_c. There is no comparable way of determining the appropriate value of κ_B for testing the boson theory. Mancini *et al.* recently have compared boson-theory results with experimental results for niobium.[44] They chose κ_B and δ to obtain the best overall agreement between theory and experiment. We have simply reproduced their theoretical results here.

II. EXPERIMENTAL METHOD

A. Sample preparation and characterization

The niobium crystal was grown by zone refining an arc-cast rod. After the first zone passes were completed for purification, the 1-cm rod was thickened during one pass to its final diameter of about 15 mm. There was one final zone pass of the 15-mm rod to improve the crystal quality. Using neutron tomography,[45] a section of the rod was selected for its crystalline quality. A sphere was spark cut from the selected portion. After the spark damage was removed by etching, the sphere was lapped to its final nearly perfect spherical shape. It was necessary to etch the sample again to remove about 50 μm of surface layer damaged by the lapping process. The sample was then annealed at 2200 °C for 50 hours in a vacuum that was better than 2×10^{-10} Torr at the end of 50 hours. Finally, the sample was heated to 400 °C for five minutes in an oxygen atmosphere. This last step is known empirically to reduce the surface barrier of niobium samples without altering the purity of the material in the bulk.[46] The final diameter of the sphere was 13 mm, and its eccentricity was found to be less than 0.035. Hereafter, this sample will be referred to as Nb-1.

A second sphere (Nb-2) was cut from the same rod, and a third sphere was cut from another single-crystal rod prepared at a different time. A few measurements made on these other samples showed slight variations that will be described later. All three samples were prepared by identical procedures, except that Nb-2 was not lapped; therefore, it showed a larger deviation from perfect spherical geometry.

The resistivity of each sample was measured in zero field just above its superconducting transition temperature by a mutual-inductance technique.[47] The resistivity of Nb-1 was found to be 32 nΩ-cm, which corresponds to a residual resistivity ratio of $\rho(295\text{ K})/\rho(10\text{ K}) = 450$. For the third sample men-

tioned above, $\rho(295\text{ K})/\rho(10\text{ K}) = 690$. With the exception of a few qualitative comparisons, only data on Nb-1 are reported in this paper.

B. Measurement technique

The magnetization was measured by a field-sweep technique. The apparatus is shown schematically in Fig. 2(a). The sample was placed in one of two identical pickup coils connected in series opposition. The sample and both coils were situated in the uniform-field region of a sixth-order superconducting solenoid. The current through the solenoid was ramped at a constant rate from below $\frac{2}{3}H_{c1}$ to above H_{c2}. Then the current was ramped down at the same constant rate to below $\frac{2}{3}H_{c1}$. The voltage induced in the pickup coils, which was just proportional to dM/dH_a, and the current through the superconducting magnet were simultaneously plotted on an x-y recorder and digitized and stored by a programmable data-acquisition system. Typically, about 80 points were stored digitally in the field range $\frac{2}{3}H_{c1} + \frac{1}{3}B_0 < H_a < H_{c2}$ and another ten points for $H_a > H_{c2}$ for each direction of field sweep. Because of the large sample size and its high conductivity, the magnetic-diffusion time was rather long, and sweep rates had to be kept below 1.5 Oe/sec (0.4 Oe/sec at temperatures above 7.5 K). The digitally stored data were later numerically integrated to obtain the magnetization and Gibbs free energy. Since the data we obtained were a slowly varying and nearly nonhysteretic function of magnetic field in the mixed state, only the mixed-state data (i.e., $H_2 \leq H_a \leq H_{c2}$) were integrated. The equilibrium magnetization curves for $H_a < H_2$ were constructed. In this way, we avoided a number of problems: (i) The rapid variation of the signal with field at H_1 and H_2 would make accurate numerical integration difficult. (ii) The signal was much noisier in the IMS than in the mixed state. (iii) The signal was history dependent in the IMS.

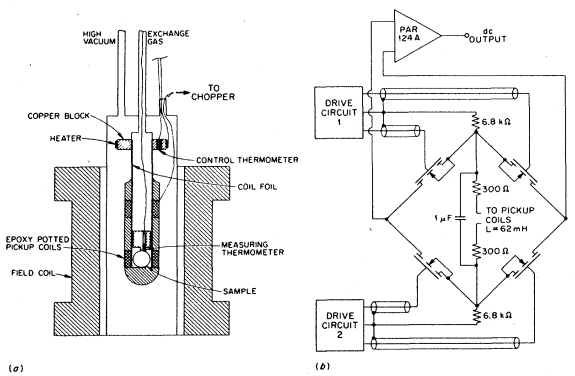

FIG. 2. (a) Experimental apparatus for measuring magnetization. (b) Schematic diagram of the MOSFET chopper. The MOSFET's are type MFE 3002.

C. dc amplifier

In order to amplify the low-level dc voltage induced in the pickup coils, we used a technique similar to that developed by Younge and Harper.[48] A metal-oxide-semiconductor field-effect transistor (MOSFET) signal chopper located in the liquid-helium bath chopped the dc voltage. The resulting ac signal was amplified and synchronously detected by a PAR 124A lock-in amplifier. This technique provided good dc stability as well as good noise immunity and relatively fast response.

A schematic of the MOSFET chopper is shown in Fig. 2(b). The isolated drive circuits each provided 0-to-15 V square-wave signals of opposite phase to turn on the four MOSFET's in pairs. The ac signal at the input to the preamp was a square wave with an amplitude equal to the dc voltage induced in the pickup coils. We used a high-input-impedance preamp to avoid field distortions arising from currents flowing in the pickup coils. A square-wave generator was the primary timing source; it drove the reference circuit of the lock-in amplifier, and it triggered the chopper drive circuits through optical isolators.

Essential to the performance of the chopper is the high degree of isolation between the low-level signal circuit and the chopper drive circuit. Without this isolation, one observes large chopping spikes that arise from currents required to charge the gate-to-source and gate-to-substrate capacitance of the MOSFET's. The optical isolators and the high-impedance input to the PAR 119 preamp prevent these charging currents from flowing in the low-level signal circuit.

Our relatively high-impedance signal source posed a more difficult problem for the signal chopper than was encountered in the earlier design, which was used to amplify thermocouple voltages.[48] (The self-inductance of our pickup coils was 62 mH.) Since a small portion of the charging currents still must flow through the signal source, we found it necessary to short-circuit these transient currents by connecting a capacitor in parallel with the pickup coil. The resistors in series with the pickup coil damped the resulting ringing. Values of the components were chosen to minimize the contribution of the switching transients to the apparent dc voltage. The ringing frequency was much higher than the chopping frequency. The damping time constant was longer than one cycle of the ringing frequency but much shorter than one half cycle of the chopping frequency.

In nearly all of the measurements, we used a chopping frequency of 47 Hz, no ac signal filtering, and a 300-msec, 12-db-per-octave dc output filter in the lock-in amplifier. At these settings, both thermal noise and the switching transients were negligible. The primary source of noise was variations in flux motion in the sample.

D. Temperature control and measurement

As shown in Fig. 2(a), the sample was placed in a cylindrical sample chamber whose wall was molded of Emerson & Cuming Stycast 2850 GT. The pickup coils were potted within this wall. Coil foil made from No. 30 copper wire was molded into the inner surface of the epoxy wall, and the sample chamber was filled with helium to insure that the entire sample chamber remained at a uniform temperature. A high-vacuum space isolated the sample chamber from the liquid-helium bath. Temperature control was accomplished by electronically regulating the power supplied to a heater mounted on a copper block near the top of the sample chamber. The control thermometer was a 100-Ω carbon resistor mounted in the copper block. We measured the temperature by using a calibrated germanium resistance thermometer, which was in contact with the sample. Cooling took place mainly through a copper wire connecting the copper block with the top flange of the vacuum can. When the sample temperature was below 4.3 K, the pressure over the liquid-helium bath was regulated to keep the bath temperature about 0.1 K below the sample temperature.

E. Sample alignment

In order to maintain alignment of the appropriate crystal axis with the magnetic field, the sample was mounted on a cylindrical post that fit closely inside the chamber. The initial orientation of the sample was accomplished by mounting it on a goniometer and obtaining successive x-ray Laue patterns while adjusting the goniometer. When the desired orientation was obtained, the goniometer and the cylindrical post were mounted in a lathe. The sample was glued to the post and then removed from the goniometer.

While alignment could be maintained to within 0.5° in transferring the sample to the post, the sample chamber could not be aligned with the magnetic field to better than about 2–3°. Since our interest was primarily in the three high-symmetry orientations, this uncertainty of 3° in the alignment was acceptable. However, a more elaborate orientation scheme would be required to investigate off-symmetry orientations.

F. Magnetic-field measurement and control

The magnetic field was generated by a sixth-order superconducting solenoid. A Kepco dc power supply, which was controlled by a specially constructed ramp generator, supplied current to the magnet. The highly capacitive output impedance of the power supply, which is typical of high-current dc supplies, gave rise to ringing currents in the magnet. Introducing more gain into the control loop of the power supply (to increase the effective output resistance) proved to be an unsatisfactory solution because the magnet current became too noisy for our measurements. It was necessary to overdamp the oscillations by (i) removing some of the capacitance across the power-supply output, (ii) adding resistance in series with the magnet, and (iii) increasing the load by placing a resistor across the power-supply output in parallel with the magnet and the series resistor. As a result of these modifications, the power supply responded only slowly to the control voltage, but after some 10 sec after the ramp generator was started, the magnet current ramped quietly at a constant rate.

During the measurements of dM/dH_a, the field was determined by measuring the voltage drop across a 0.1-ohm standard resistor that was wired in series with the superconducting solenoid. To calibrate the solenoid, we compared it with a previously calibrated solenoid by measuring the magnetoresistance of platinum wire. The precision of our magnetic-field measurements was limited by field due to trapped flux in the superconducting windings. This trapped field was measured to be 5.6 Oe on the average (after raising the field to several kOe) with an uncertainty of about 3 Oe, depending on field history. There was an additional uncertainty of about 0.2% of H_{c2} (0.5 mm) in reading the critical fields off the x-y recordings.

III. RESULTS

A. dM/dH_a

A typical dM/dH_a plot is shown in Fig. 3, along with the magnetization curve that is obtained by numerical integration. The data show all the qualitative features of the idealized plot of Fig. 1. The Meissner state, the IMS, the mixed state, and the normal state are clearly distinguishable regions of the dM/dH_a curve. As noted above, the mixed-state region is smooth and shows almost no hysteresis; therefore, it is the most appropriate region to use to infer equilibrium properties. Hysteretic effects that appear clearly in the dM/dH_a plot between H_1 and H_2 are visible in the $M(H_a)$ plot only near H_1.

The region near H_{c2} is shown in the inset with the vertical scale expanded by a factor of 10. The transition takes place within 20 Oe (10% to 90%), allowing H_{c2} to be determined to this precision. We took H_{c2} to be the midpoint of the transition. The slope of the magnetization at H_{c2} was determined by extrapolating the measured curve to the midpoint of the transition. As the data show, dM/dH_a varies with field over the whole mixed state, so that earlier experiments,[3–6] in which dM/dH_a at H_{c2} was evaluated by fitting a straight line to the magnetization curve near H_{c2}, must have produced systematically high values of this

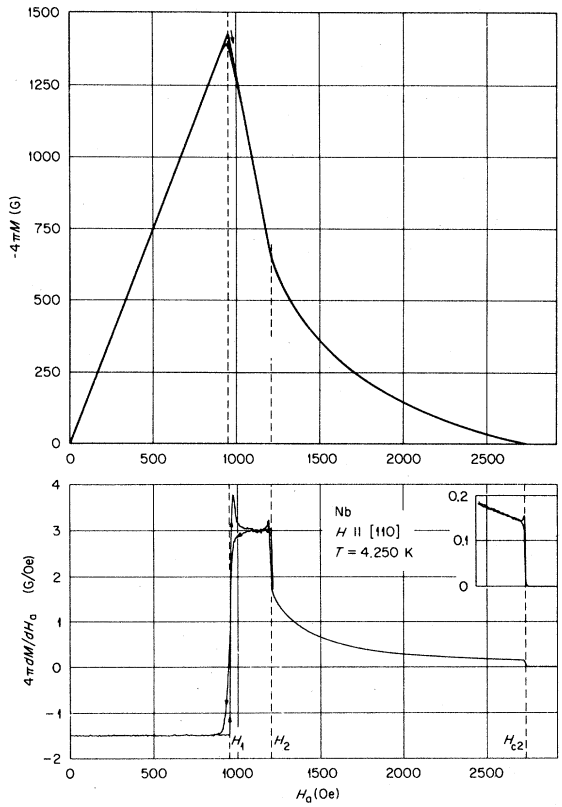

FIG. 3 Experimentally measured dM/dH_a and $M(H_a)$ obtained by numerical integration.

quantity. A narrow peak in the dM/dH_a data was observed just below H_{c2} in increasing field, and a corresponding dip was observed in decreasing field. The entire peak occurs within 10 Oe of the midpoint of the transition. Its presence implies a field-independent hysteresis in the mixed-state magnetization of about 3 G.

The transition at H_2 between the mixed state and the intermediate mixed state was also about 20 Oe wide; however, the transition began at the same field (to within our field resolution of about 5 Oe) in both increasing and decreasing field. Therefore, we took the field at which the transition started to be the best measure of H_2.

The start of the transition at H_1 in increasing field defined accurately the field at which flux first entered the sample. We take this field to be H_1 for the purposes of discussion of the data. Below, we show that H_1 is slightly larger than $\frac{2}{3}H_{c1}$. The transition in decreasing field was too broad to serve as a useful measure of H_{c1}.

In order to test the importance of dynamic effects on the transitions, we made a brief study of the sweep-rate dependence of the dM/dH_a curve. While the sweep rate had little effect on the transition at H_{c2}, the width of the transitions at H_2 (in increasing and decreasing field) and at H_1 (in increasing field only) increased with sweep rate. The peak that occurred near H_2 in decreasing field disappeared into the noise as the sweep rate was decreased, suggesting that it was entirely a dynamic effect. In contrast, as the sweep rate was decreased, the peak that occurred near H_1 in increasing field became narrower and higher, while the area under the peak approached a constant value. This behavior suggests that the Meissner state is metastable at H_1, as indeed we found from other, more conclusive, evidence discussed below.

Although the data at 4.25 K were representative of data obtained over a wide range of temperatures, some changes in the dM/dH_a curves were noted both at the lowest temperatures and near T_c. The peak near H_{c2} decreased in size as the temperature was raised and was absent above 5 K. The data showed greater hysteresis, and the transition at H_2 was less well defined below 2 K. The discontinuity in dM/dH_a at H_2 decreased with increasing temperature and became unobservably small at 8.3 K. The intermediate mixed state could not be observed above 8.7 K. These last two observations could be interpreted to mean that the first-order transition at H_{c1} in niobium becomes second order sufficiently close to T_c. On the other hand, it must be recognized that good measurements were increasingly difficult to obtain above 8 K. The compression of the entire magnetization curve into a small field range required the use of a slow sweep rate and a corresponding reduction in the signal-to-noise ratio. Even at our slowest sweep rate of 0.4 Oe/sec, dynamic broadening of the transitions was a significant problem near T_c.

B. Low-field results

The lower critical field H_{c1} is the value of the equilibrium field H at which the mixed state and the Meissner state are in equilibrium. It depends both on temperature and on sample orientation. We determined H_{c1} from our measurements of H_2 and $M(H_a)$ by using the relation

$$H_{c1} = H_2 - \tfrac{4}{3}\pi M(H_2) \quad . \tag{18}$$

The field of first flux entry, H_1, proved to be an unreliable measure of H_{c1} because the Meissner state superheated to applied fields slightly in excess of $\frac{2}{3}H_{c1}$.

Measured values of the lower critical field normalized by the thermodynamic critical field are plotted in Fig. 4. For comparison with our data, we have also plotted the smoothed results reported by Finnemore, Stromberg, and Swenson,[3] the Gor'kov-theory results of Brandt[37] for $\kappa = 0.773$ (the measured value for this

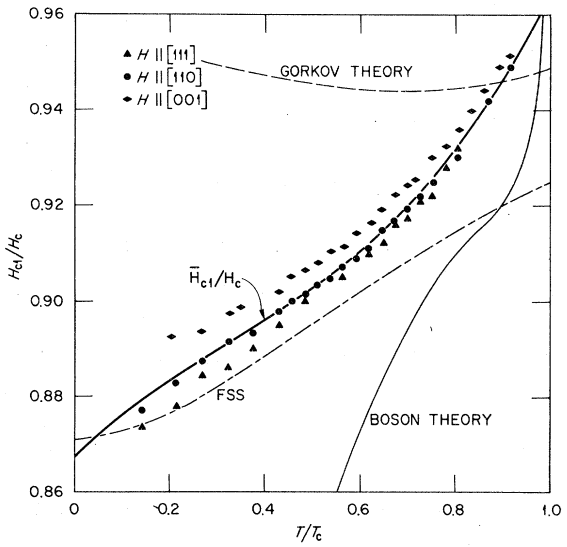

FIG. 4. Temperature dependence of the lower critical field H_{c1} normalized by the thermodynamic critical field H_c. Our data and our smoothed, spatially averaged results are compared with the smoothed results of Ref. 3 (FSS) and with the theoretical results of Refs. 37 (Gor'kov theory) and 44 (boson theory).

sample), and the boson-theory results of Mancini, Tachiki, and Umezawa.[44] The field H_{c1}^* in equilibrium with an isolated fluxoid, which was calculated by Pesch and Kramer,[36] lies almost entirely off scale above this plot. At low temperature, the Pesch and Kramer value of H_{c1}^*/H_c is nearly 1 for $\kappa=0.773$ and decreases to Brandt's result at T_c. The boson-theory result is also a calculation of H_{c1}^*, but it lies below our data, falling to only 60% of our measured H_{c1}/H_c at low temperatures.

Near T_c, Gor'kov theory simplifies to Ginzburg-Landau theory.[28] Anisotropy must disappear, and the Brandt[37] and the Pesch and Kramer[36] values of H_{c1}/H_c must coincide with the Ginzburg-Landau value calculated numerically for small κ by Harden and Arp.[49] For $\kappa=0.773$, the Ginzburg-Landau result is $H_{c1}/H_c=0.949$. This value is slightly smaller than the extrapolated value $H_{c1}/H_c=C_{00}=0.966$ obtained from our data [see Eq. (19) below]. Conversely, $H_{c1}/H_c=0.966$ yields $\kappa=0.75$ according to Ginzburg-Landau theory.

The anisotropy in H_{c1}, although small, is clearly evident in Fig. 4. We fitted the expression

$$F(t,\vec{e})=C_{00}+\sum_{n=1}^{N}\sum_{l=0,4,6}C_{nl}(1-t)^n\mathcal{K}_l(\vec{e}) \quad (19)$$

to the experimental values of H_{c1}/H_c. Here $N=3$, $t=T/T_c$ is the reduced temperature, and $\mathcal{K}_l(\vec{e})$ is the cubic harmonic of angular momentum l evaluated in the direction of the applied magnetic field, $\vec{e}=\vec{H}_a/H_a$.[50] In terms of the direction cosines, α, β, and γ (with respect to the crystal directions [100], [010], and [001]),

$$\mathcal{K}_0=1 \ , \quad (20a)$$

$$\mathcal{K}_4=\tfrac{5}{4}\sqrt{21}(\alpha^4+\beta^4+\gamma^4-\tfrac{3}{5}) \ , \quad (20b)$$

$$\mathcal{K}_6=\tfrac{231}{8}\sqrt{26}[\alpha^2\beta^2\gamma^2+\tfrac{1}{22}(\alpha^4+\beta^4+\gamma^4-\tfrac{3}{5})-\tfrac{1}{105}] \ . \quad (20c)$$

The temperature dependence of the spatially averaged $\bar{H}_{c1}/H_c$ is plotted in Fig. 4, and the temperature dependences of the coefficient of the cubic harmonics are plotted in Fig. 5. The $l=6$ term is small over the whole temperature range investigated; therefore, the values obtained should not be considered significant. The coefficients obtained from the neutron-diffraction measurements of H_{c1} made at 4.3 K (see Fig. 6 of II) are shown in Fig. 5 for comparison. The theoretical anisotropy of H_{c1}^* near T_c is

$$\frac{\Delta H_{c1}^*}{\bar{H}_{c1}^*}=-0.281\left(\frac{\langle v_x^4\rangle}{\langle v^4\rangle}-0.2\right)\left(1-\frac{T}{T_c}\right)\mathcal{K}_4(\hat{H}) \quad (21)$$

for $\kappa=0.773$.[40] Here v is the Fermi velocity, v_x is the component of the Fermi velocity projected onto the [100] crystal direction, and $\langle\cdots\rangle$ indicates an average over the Fermi surface. Identifying H_{c1} with H_{c1}^*, we obtain from our data $\langle v_x^4\rangle/\langle v^4\rangle-0.2=-0.037$.

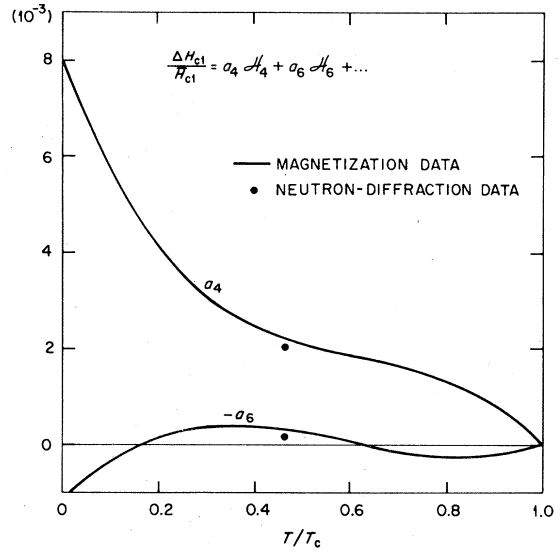

FIG. 5. Temperature dependences of the cubic-harmonic coefficients for H_{c1}.

In Fig. 6 we have plotted $\frac{3}{2}H_1$; that is, the field of first flux entry scaled up to compare with H_{c1}. The curves corresponding to the least-squares fit of H_{c1}/H_c for each of the three orientations are shown for comparison. Although the effects are almost obscured by the scatter in these data, two qualitative observations may be made. First, $\frac{3}{2}H_1$ is systematically larger than H_{c1}, indicating a superheating of the Meissner state. Second, $\frac{3}{2}H_1$ is anisotropic with a different anisotropy than H_{c1}. The superheating is most pronounced for $H \| [111]$, while there is no superheating evident for $H \| [110]$. Since one expects the attractive fluxoid–fluxoid interaction to be strongly anisotropic on theoretical grounds,[19,51] that effect (i.e., the anisotropy of $H_{c1}^* - H_{c1}$) may account for this observation. One also expects a surface barrier to be anisotropic because the interaction between a fluxoid and the surface currents depends on the (anisotropic) penetration depth.[22] However, it would seem unlikely that either effect would go to zero in one orientation.

Surface roughness reduces the superheating field and may be distributed unevenly in such a way as to produce a spurious anisotropy of the superheating field. For this reason, it is unlikely that H_1 represents an ideal superheating field. The quantity $\frac{3}{2}H_1 - H_{c1}$ is smaller than $H_{c1}^* - H_{c1}$ calculated on the basis of Gor'kov theory, and it is strongly anisotropic.

The equilibrium flux density B_0 at H_{c1} was determined from our measurements of H_2 and $M(H_2)$ by using the relation

$$B_0 = H_2 + \tfrac{8}{3}\pi M(H_2) \quad . \tag{22}$$

The anisotropy in B_0 is smaller than the scatter in our data and could not be determined from the magnetization measurements. Therefore, B_0/H_c is plotted in Fig. 7 for one orientation only. The anisotropy in B_0 is discussed in II, where the inherently more accurate neutron-diffraction results are reported. For comparison, we have plotted the neutron-diffraction measurements of B_0 for the same orientation, the measurements of Kumpf,[8] Brandt's calculated B_0/H_c,[37] and the boson-theory result of Mancini *et al.*[44] While there are small differences in measurements of B_0 from sample to sample, the measurements lie well below the Gor'kov-theory result and well above the boson-theory result. As in the plot of H_{c1}/H_c, we assumed $\kappa = 0.773$ in the Gor'kov theory and $\kappa_B = 0.75$ in the boson theory.

The field derivative of the magnetization at H_2 can be read directly from the x-y recordings. We have converted those measurements to values of $(dH/dB)|_{H_{c1}}$, which are plotted in Fig. 8. Again, the data for only one orientation are plotted because no anisotropy of this quantity could be observed. Combined with the measurements of B_0 and H_{c1}, the measurement of $(dH/dB)|_{H_{c1}}$ provides information about the degree of nonlinearity in the thermodynamic function $f(\vec{B})$ at low B. Theoretically, both B_0/H_c and $(dH/dB)|_{H_{c1}}$ should approach zero as nonlocal electrodynamic effects become unimportant for T near T_c. Near T_c, $(dH/dB)|_{H_{c1}}$ appears to drop to zero while B_0/H_c is still finite, indicating that $f(\vec{B})$ is nearly linear in B over the finite range B_0. However, the uncertainty in the measurements gets

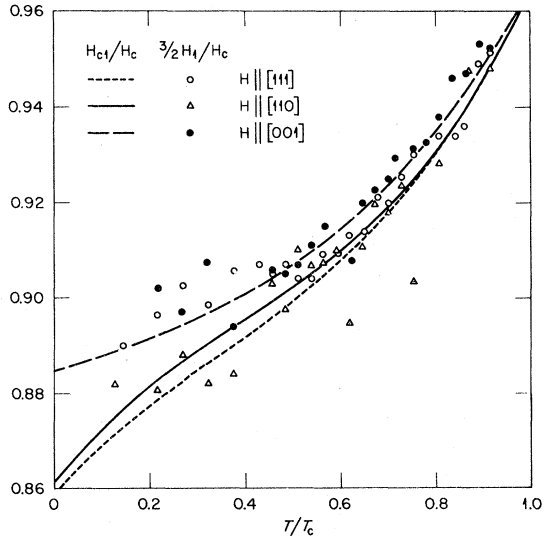

FIG. 6. Comparison between $\frac{3}{2}H_1$ and the smoothed H_{c1} data (solid curves).

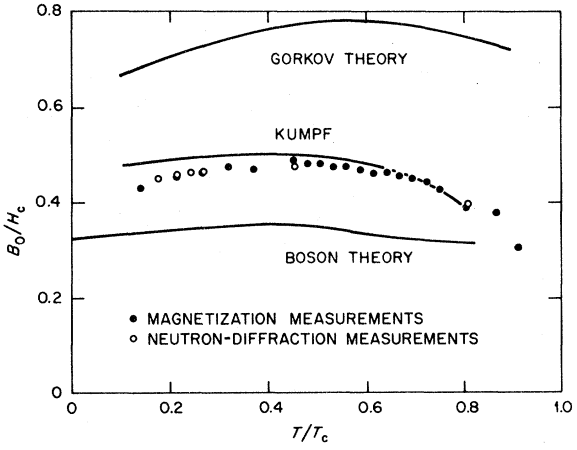

FIG. 7. Temperature dependence of the equilibrium flux density B_0 at H_{c1} normalized by the thermodynamic critical field H_c for $H \| [110]$. Our data (points) are compared with the smoothed results of Ref. 8 (Kumpf) and with the theoretical results of Refs. 37 (Gor'kov theory) and 44 (boson theory).

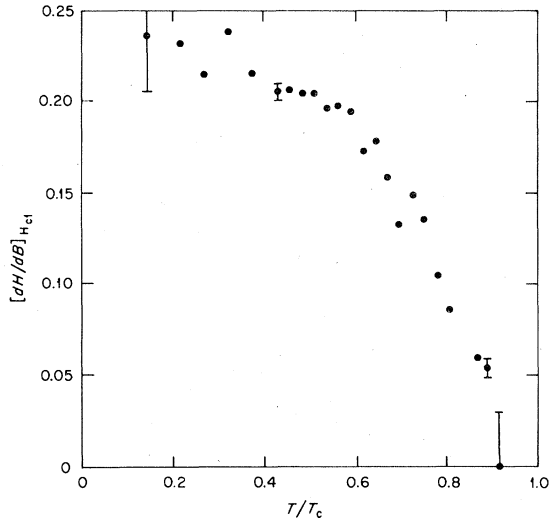

FIG. 8. Temperature dependence of the derivative dH/dB at H_{c1} for $H \| [110]$.

large near T_c, as indicated by the error bars. It is difficult even to rule out a linear relation between $(dH/dB)|_{H_{c1}}$ and $(T_c - T)$.

D. High-field results

The data obtained at the upper critical field H_{c2} are presented in Fig. 9 as values of the parameters κ_1 and κ_2, which are defined by

$$\kappa_1 = H_{c2}/\sqrt{2}H_c \ , \tag{23}$$

$$\kappa_2 = \left\{\frac{1}{2}\left[1-(3\beta)^{-1}+\left(4\pi\beta\frac{dM}{dH_a}\right)\Big|_{H_{c2}}^{-1}\right]\right\}^{1/2} \ , \tag{24}$$

where we assumed $\beta = 1.1596$, as for a hexagonal fluxoid lattice. The experimental values of κ_1 for each orientation were fitted to a quadratic polynomial in $(1 - T/T_c)$. The value of κ_1 averaged over all crystal orientations was determined from the three polynomials, and the result is shown as the solid curve labeled $\bar{\kappa}_1/\kappa$. The experimental values of κ_2 were fitted to an expression of the form given by Eq. (19) with $N = 4$. The solid curve labeled $\bar{\kappa}_2/\kappa$ is the spatially averaged value of κ_2/κ [i.e., the coefficient of $H_0(\vec{e})$].

In the absence of a realistic microscopic theory of the mixed state below H_{c2}, Eq. (24) must be construed as an arbitrary experimental definition. Equation (24) coincides with the interpretation of earlier experiments, and κ_2 as defined by Eq. (24) approaches κ as $T \to T_c$. In Gor'kov theory

$$4\pi\left(\frac{dM}{dH_a}\right)\Big|_{H_{c2}} = [\beta(2\kappa_2^2 - \eta) + \tfrac{1}{3}]^{-1} \ , \tag{25}$$

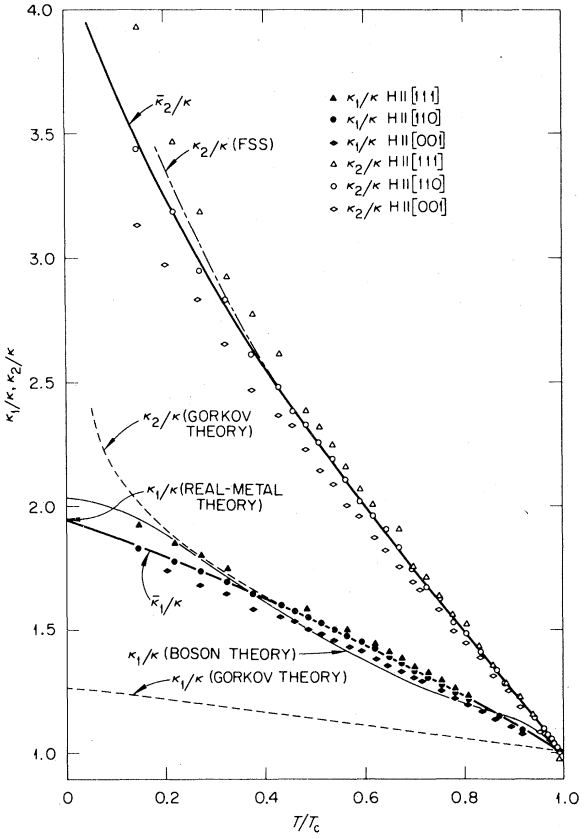

FIG. 9. Temperature dependences of the generalized Ginzburg-Landau parameters κ_1 and κ_2. Our data and our smoothed, spatially averaged results are compared with the smoothed results of Ref. 3 (FSS), with the Gor'kov-theory results of Ref. 32, with the boson-theory results of Ref. 44, and with the zero-temperature calculations of Refs. 55 and 56, which include real-metal effects.

where η is a temperature-dependent function that decrease monotonically with increasing temperature to $\eta = 1$ at T_c, and β is a fluxoid-lattice sum that would increase from the value $\beta = 1.1596$ if the lattice were distorted from hexagonal symmetry. Since Gor'kov theory is isotropic, it cannot account for an anisotropic $f(\vec{B})$, for misalignment between $\vec{M}$ and $\vec{H}_a$ (in a sphere), or for the nonhexagonal fluxoid lattices that we observe.[1]

Our result for $\bar{\kappa}_1$ is indistinguishable from the smoothed results of Finnemore, Stromberg, and Swenson (FSS).[3] However, they obtain slightly higher values of $\bar{\kappa}_2$ at low temperatures. From the extrapolations to T_c of the least-squares fits to these data, we obtain $\kappa = 0.773 \pm 0.003$. For ideally pure niobium we find $\kappa_0 = 0.75$ by using Goodman's[52] approximate relation, $\kappa = \kappa_0 + 7.5 \times 10^3\sqrt{\gamma\rho}$, the electronic specific-heat coefficient $\gamma = 7.2 \times 10^3$

erg/cm^3 K^2,[53] and our measurement of the resistivity $\rho = 32$ nΩcm. This value is 4% lower than the value of κ measured by Finnemore, Stromberg, and Swenson[3] in spite of the high purity they report. Our value of κ_0 is also 8% lower than reported by French[4] and 7% higher than reported by Alekseyevskiy *et al.*[11] The reason for these discrepancies is unclear. They may arise from (i) difficulty with extrapolating lower-temperature data to T_c, (ii) difficulty with the identification of H_{c2} in inhomogeneous samples or samples with strong surface-sheath currents, (iii) uncertainty in the measurements of H_c in less reversible samples, or (iv) difficulty with extrapolating resistivity measurements on a high-purity sample to zero field and zero temperature.

It is well known that κ_1/κ and κ_2/κ calculated on the basis of Gor'kov theory fall well below the experimental results for niobium. We have presented only the simplest possible comparison with Gor'kov theory in Fig. 9. Two details of the theory have been neglected; they both make the agreement slightly worse. First, the electron scattering by impurities reduces both κ_1/κ and κ_2/κ from the clean-limit results, which are shown. Second, the correct theoretical expression, Eq. (25), predicts a larger value of $(dM/dH_a)|_{H_{c2}}$ than one obtains by approximating $\eta \simeq 1$ as we did when deriving κ_2 from the data. Since the theoretical value of $(dM/dH_a)|_{H_{c2}}$ is already too large, our approximation artificially improves the agreement between Gor'kov theory and experiment.

The boson-theory result for κ_1/κ agrees much more closely with the experimental result over the whole temperature range, but that agreement is due to the fact that two parameters, $\delta = H_{c2}(0)/H_c(0)$ and κ_B could be adjusted instead of just one as in Gor'kov theory. The boson-theory curve shows more structure than the experimental results; for example, the theoretical curve drops more sharply near T_c. The reason for this discrepancy is unclear at the present time.

Since the anisotropy in bulk superconducting properties of a cubic crystal is a nonlocal phenomenon, the anisotropy must vanish near T_c. No anisotropy of H_{c2} was observable above 9 K. We found $T_c(dH_{c2}/dT)|_{T_c} = 4326$ Oe by fitting a straight line to the data above 9 K. The best-fit line intersected the $H = 0$ axis with 0.001 K of $T_c = 9.297$ K, which was determined by observing the temperature at which the last trace of superconductivity disappeared. Ginzburg-Landau theory may be used to calculate the limiting temperature dependence of the superconducting penetration depth by using the relation

$$\lambda^2 = \sqrt{2}\phi_0\kappa_0/4\pi H_c \ . \tag{26}$$

Our measurements yield $\lambda = 210$ Å$(1 - T/T_c)^{-1/2}$ near T_c. This result can be compared with the direct measurement by Varmazis and Strongin[54] of $\lambda = 223$ Å$(1 - T/T_c)^{-1/2}$.

Our measurements of the relative anisotropy of H_{c2} can be compared directly with previous measurements. We derived the parameters $\bar{H}_{c2}$, a_4, and a_6 in the formula

$$\Delta H_{c2} = H_{c2} - \bar{H}_{c2} = \bar{H}_{c2}(a_4\mathcal{K}_4 + a_6\mathcal{K}_6) \tag{27}$$

from individual measurements of H_{c2} at the same temperature for the three high-symmetry crystal orientations. Our results for a_4 and a_6 are compared with the values obtained from two previous studies[16,18] in Fig. 10. Although our method of determining a_4 and a_6 is much cruder than was used in the previous studies, the results compare well. It follows that the values of microscopic anisotropy parameters, which were derived from the data of Seidl *et al.*[18] are consistent with our measurements.

We have plotted in Fig. 11 the parameters describing the relative anisotropy of κ_2. It appears that not only $\bar{\kappa}_2$ but also $\Delta\kappa_2/\bar{\kappa}_2$ diverges at low temperature. (Actually the theoretical divergence of κ_2 is removed by a finite electron mean free path. Presumably, we would see $\bar{\kappa}_2$ and $\Delta\kappa_2/\bar{\kappa}_2$ level off at sufficiently low temperature.) Comparing Figs. 10 and 11, it is clear that $\Delta\kappa_2/\bar{\kappa}_2 > \Delta\kappa_1/\bar{\kappa}_1$ over the whole temperature range and that the ratio of the two relative anisotropies varies with temperature. Although our values of κ_2 are larger than those reported by Williams and Court[6] and Gough[5] for single crystals of niobium, the relative anisotropy agrees well with both previous measurements. Holzhäuser found different results for the relative anisotropy of κ_2 by deriving it from his torque measurements.[23] However, the power-series expansion of the torque in Ref. 23 is incomplete. It includes the terms of order $(1 - H/H_{c2})^2$ that depend on the anisotropy of κ_2 but not the other terms of the same order, that depend on the anisotropy of H_{c2}.

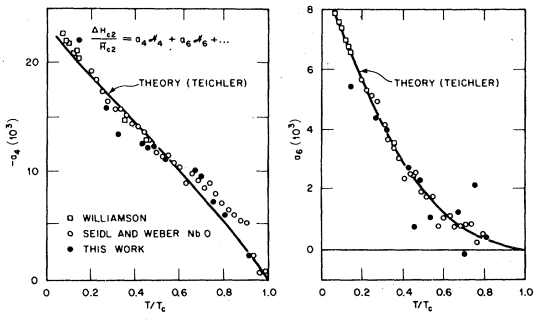

FIG. 10. Temperature dependences of the cubic-harmonic coefficients for H_{c2}. Our data are compared with the data of Williamson (Ref. 16) and Seidl *et al.* (Ref. 18), and with the theoretical curve of Teichler, which was fit to the data of Seidl *et al.* (Ref. 18).

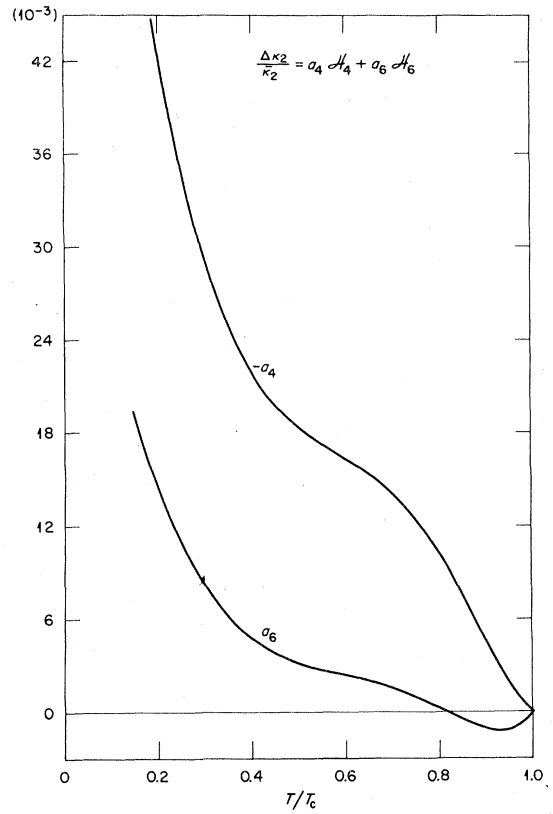

FIG. 11. Temperature dependences of the cubic-harmonic coefficients for κ_2.

The theoretical relative anisotropy of κ_2 near T_c is

$$\frac{\Delta\kappa_2}{\kappa}=1.924\left[\frac{\langle v_x^4\rangle-0.2\langle v^4\rangle}{\langle v^2\rangle^2}\right]\left[1-\frac{T}{T_c}\right]\mathcal{K}_4(\hat{H}) \tag{28}$$

for $\kappa=0.773$.[42] Here κ_2 is the parameter defined by Eq. (24) for $\hat{H}$ in one of the high-symmetry crystal directions. Equation (28) includes anisotropy in both κ_2 and η of Ref. 42. From our data we find $(\langle v_x^4\rangle-0.2\langle v^4\rangle)/\langle v^2\rangle^2=-0.040$. This value is reasonably consistent with the value -0.044 given in Ref. 42, with the result $(\langle v_x^4\rangle/\langle v^4\rangle-0.2)=-0.037$ deduced from our H_{c1} measurements and the comparable results

$$\frac{4}{15\sqrt{21}}\left\langle\left[1+2\frac{\delta v^2}{\langle v^2\rangle}\right]\mathcal{K}_4(\vec{v})\right\rangle=-0.029$$

deduced by Seidl *et al.*,[18] and -0.025 calculated by Butler by using band-theory results for $\vec{v}$.[55] These three quantities differ by terms of order $\langle v^4\rangle/\langle v^2\rangle^2-1$, which is small in the limit of small anisotropy in the sense of Teichler.[39]

The variation in Fermi velocity over the Fermi surface enhances $\bar{H}_{c2}$ and $\bar{\kappa}_2$ over the Gor'kov-theory results by an amount proportional to $\langle v^4\rangle/\langle v^2\rangle^2-1$. Near T_c,

$$\bar{H}_{c2}=\left[\frac{dH_{c2}}{dT}\right]\Big|_{T_c}(T_c-T)\times\left\{1+\left[1-\frac{T}{T_c}\right]\left[0.135+1.635\left[\frac{\langle v^4\rangle}{\langle v^2\rangle^2}-1\right]\right]\right\}, \tag{29}$$

$$\frac{\bar{\kappa}_2}{\kappa}=1+\left[1-\frac{T}{T_c}\right]\left[1.133+3.041\left[\frac{\langle v^4\rangle}{\langle v^2\rangle^2}-1\right]\right], \tag{30}$$

for $\kappa=0.773$.[42] Again, κ_2 is defined by Eq. (24). From our data for H_{c2}, we find $\langle v^4\rangle/\langle v^2\rangle^2=1.30$, and from our data for κ_2 we find $\langle v^4\rangle/\langle v^2\rangle^2=1.46$. Butler[55] calculates $\langle v^4\rangle/\langle v^2\rangle^2=1.58$. The agreement among these results is less than satisfactory; the difference may arise from neglecting terms of higher order in $(1-T/T_c)$ in our data analysis, or it may arise from neglecting other real-metal effects in the theory. At $T=0$, the enhancement of H_{c2} has been calculated by Mattheiss[56] and recently by Butler[55] by using band-theory results for $\vec{v}$ and the formula derived by Hohenberg and Werthamer.[38] The two theoretical results are indicated in Fig. 9. They are both identical to our extrapolation of the data to $T=0$.

The limiting misalignment angle between the magnetization and the field and the limiting field dependence of the torque on a sample at H_{c2} are related to the anisotropy of H_{c2} by Eq. (17). We can make a direct comparison between the measurements of H_{c2} and the torque measurements. Using the 4.2-K values, $a_4=-0.133$ and $a_6=0.0024$ from Fig. 10, we find that the maximum misalignment angle $\epsilon=5.1°$ occurs for $\vec{H}$ at an angle of 30° from the [001] direction in the (110) plane (and equivalent directions). The torque per unit volume is

$$|\vec{M}\times\vec{H}|=\left[\frac{H_{c2}^2\sin\epsilon}{4\pi\beta(2\kappa_2^2-1)}\right]\left[1-\frac{H}{H_{c2}}\right]$$
$$=7830\left[1-\frac{H}{H_{c2}}\right]\ \text{erg/cm}^3\ .$$

These results appear to be larger than those reported by Holzhäuser[23] and by Schneider *et al.*[24] The samples that have been studied appear to be less reversible than our sample, making the measurement of the equilibrium torque difficult and possible producing the observed discrepancy. The discrepancy may also be due to the fact that the torque depends nonlinearly on field even close to H_{c2}. A similar comparison can be made between the anisotropy of H_{c1} and the torque in the intermediate mixed state. Those results will be discussed in II.

IV. SUMMARY AND CONCLUSIONS

The equilibrium magnetic properties of superconducting niobium are now demonstrably well known. With only a few exceptions, the bulk-magnetization measurements reported here are consistent with earlier measurements where they overlap. Moreover, the bulk-magnetization measurements are consistent with the microscopic measurements reported in II. In contrast, the theoretical understanding of these magnetic properties is incomplete. The only exceptions are the understanding of H_c and H_{c2}. We defer discussion of realistic microscopic theories of H_c and H_{c2} to a forthcoming publication. Near T_c the anisotropy of the Fermi surface has been taken into account in calculations of H_{c1}^* and κ_2 as well as in the more nearly complete calculations of H_{c2}. The single parameter $\langle v_x^4\rangle/\langle v^4\rangle - 0.2 \simeq -0.04$ describes the relative anisotropy of H_{c1}, H_{c2}, and κ_2 near T_c to within the limits of precision of the data. Two qualifications to this conclusion are in order. First, Teichler's fitted temperature dependence of $\Delta H_{c2}/\overline{H}_{c2}$ is nonlinear in $(1 - T/T_c)$ even close to T_c; therefore, the limiting theoretical temperature dependence of the relative anisotropy of H_{c2} and perhaps of other quantities may not be closely related to the experimental measurements. Second, the Fermi-surface averages entering the theoretical anisotropy of H_{c1} and of H_{c2} and κ_2 differ by the factor $\langle v^4\rangle/\langle v^2\rangle^2$, which we estimate to be about 1.5.

Near H_{c1} only isotropic, weak-coupling theory is available to compare with our data over the entire temperature range. Calculations based on Gor'kov theory give almost the observed value of H_{c1}, but they give values of B_0 that are too large by nearly a factor of 2. Although the boson-theory results for H_{c1} are worse than Gor'kov theory, at least at low temperatures, the boson-theory results for B_0 are better. In making these comparisons, we have used the numerical results of Mancini *et al.*[44] Those results are obtained after adjusting the boson-theory parameters to obtain the best agreement with experiment.

Niobium appears to obey the Ginzburg-Landau-Abrikosov theory at T_c. The extrapolation to T_c of H_{c2}/H_c and $(dM/dH)|_{H_{c2}}$ extrapolates to the values associated with $\kappa = 0.773$ to within 0.5%. The extrapolated value of H_{c1}/H_c differs by about 2% from the theoretical value for $\kappa = 0.773$. This small discrepancy could be removed, for example, by assuming that the highest-temperature measurements of H_c are systematically about 0.5% too low. Although we could not observe a finite B_0 near T_c, previous measurements[10] have indicated that B_0/H_{c2} does not go to zero at T_c as required by Ginzburg-Landau theory. Brandt has suggested that B_0/H_{c2} in fact goes to zero but only very close to T_c.[37] We could see no evidence for type-I superconductivity near T_c as reported by Alekseyevskiy *et al.*[11]

Note added in proof. We have recently become aware that K. Takanaka and T. Nagashima independently derived Eq. (17). Their work will appear in the J. Phys. Soc. Jpn.

ACKNOWLEDGMENTS

The authors are grateful to H. Harmon and Y. K. Chang for their extraordinary efforts in preparing the samples. E. H. Brandt, W. H. Butler, H. Umezawa, and M. Tachiki were most helpful by elucidating much of the theory. W. H. Butler kindly supplied us with the results of his unpublished calculations. R. H. Kernohan and C. C. Watson provided experimental assistance. This research was sponsored by the Division of Materials Science, U. S. DOE under Contract No. W-7405-eng-26 with the Union Carbide Corporation.

APPENDIX: NUMERICAL-INTEGRATION METHOD

After measuring and storing values of dM/dH_a and determining the fields H_2 and H_{c2}, the data were integrated twice between H_2 and H_{c2} to obtain $M(H_a)$ and $\int_{H_a}^{H_{c2}} M(H_a')\,dH_a'$. Each datum was first corrected for the small component of measured voltage that was due to an imbalance in the pickup coils by subtracting the average voltage measured above H_{c2}. The first integration was performed by using an adaptation of the program AVINT.[57] This program incorporates a simple data-averaging procedure into the integration. The magnetization is given by

$$M(H_a) = \int_{H_a}^{H_{c2}} M'(H_a')\,dH_a' = \sum_{\gamma=0}^{2} (\gamma+1)^{-1}\left\{\sum_{i=2}^{N}\tfrac{1}{2}(a_{\gamma,i}+a_{\gamma,i-1})(H_{a,i}^{\gamma+1}-H_{a,i-1}^{\gamma+1}) + 2a_1(H_{a,1}^{\gamma+1}-H_a^{\gamma+1}) + 2a_N(H_{c2}^{\gamma+1}-H_{a,N}^{\gamma+1})\right\}, \quad \text{(A1)}$$

where $H_{a,1} > H_a$ and $H_{a,N} < H_{c2}$, and the polynomial

$$P_i(H_a) = a_{0,i} + a_{1,i}H_a + a_{2,i}H_a^2 \quad \text{(A2)}$$

passes through the three data, $M'(H_{a,i+1})$, $M'(H_{a,i})$, and $M'(H_{a,i-1})$. The second integration was performed by

using a Hermitian formula of first order,[58]

$$\int_{H_2}^{H_{c2}} M(H_a)\, dH_a = \tfrac{1}{2}\sum_{i=1}^{N} (H_{a,i} - H_{a,i-1})\{M(H_{a,i}) + M(H_{a,i-1}) + \tfrac{1}{6}(H_{a,i} - H_{a,i-1})[M'(H_{a,i-1}) - M'(H_{a,i})]\} \quad . \quad \text{(A3)}$$

[1]D. K. Christen, H. R. Kerchner, S. T. Sekula, and P. Thorel, Phys. Rev. B 21, 102 (1980) (following paper).
[2]B. Serin, Phys. Lett. 16, 112 (1965).
[3]D. K. Finnemore, T. F. Stromberg, and C. A. Swenson, Phys. Rev. 149, 231 (1966).
[4]R. A. French, Cryogenics 8, 301 (1968).
[5]C. E. Gough, Solid State Commun. 6, 215 (1968).
[6]I. Williams and A. M. Court, Solid State Commun. 7, 169 (1969).
[7]A. Ikushima and T. Mizusaki, J. Phys. Chem. Solids 30, 873 (1969).
[8]U. Kumpf, Phys. Status Solidi B 44, 829 (1971).
[9]J. Auer and H. Ullmaier, Phys. Rev. B 7, 136 (1973).
[10]J. J. Wollan, K. W. Haas, J. R. Clem, and D. K. Finnemore, Phys. Rev. B 10, 1874 (1974).
[11]N. Ye. Alekseyevskiy, V. I. Nizhankovskiy, and K. -H. Bertel, Fiz. Met. Metalloved. 37, 63 (1974) [Phys. Met. Metallogr. (USSR) 37, 53 (1974)].
[12]The theory of the mixed state has been reviewed by A. L. Fetter and P. C. Hohenberg, in *Superconductivity,* edited by R. D. Parks (Marcel Dekker, New York, 1969), Chap. 14.
[13]D. R. Tilley, G. T. van Gurp, and C. W. Berghout, Phys. Lett. 12, 305 (1964).
[14]W. A. Reed, E. Fawcett, P. P. M. Meincke, P. C. Hohenberg, and N. R. Werthamer, in *Proceedings of the Tenth International Conference on Low-Temperature Physics, Moscow, 1966,* edited by M. P. Malkov (Prorzvodslrenno-Izdatel'skii Kombinat, V1N111, Moscow, 1967), Vol. IIA, p. 368.
[15]D. E. Farrell, B. S. Chandrasekhar, and S. Huang, Phys. Rev. 176, 562 (1969).
[16]S. J. Williamson, Phys. Rev. B 2, 3545 (1970).
[17]M. Yamamoto, N. Ohta, and T. Ohtsuka, J. Low Temp. Phys. 15, 231 (1974).
[18]E. Seidl, H. W. Weber, and H. Teichler, J. Low Temp. Phys. 30, 273 (1978).
[19]M. Tachiki (private communication).
[20]Metastable states in type-I superconductors are reviewed in F. W. Smith, A. Baratoff, and M. Cardona, Phys. Kondens. Mater. 12, 145 (1970).
[21]Fluxoid pinning has been reviewed in A. M. Campbell and J. E. Evetts, *Critical Currents in Superconductors* (Taylor and Francis, London, 1972).
[22]J. R. Clem, in *Proceedings of the Thirteenth International Conference on Low-Temperature Physics, Boulder, 1972,* edited by K. D. Timmerhaus, W. J. O'Sullivan, and E. F. Hammel (Plenum, New York, 1974), Vol. 3, p. 102.
[23]W. Holzhäuser, J. Low Temp. Phys. 24, 175 (1976).
[24]R. Schneider, J. Schelten, and C. Heiden, in *Anisotropy Effects in Superconductors,* edited by H. W. Weber (Plenum, New York, 1977), p. 177.
[25]A. A. Abrikosov, Zh. Eksp. Teor. Fiz. 32, 1442 (1957) [Sov. Phys. JETP 5, 1174 (1957)].
[26]V. L. Ginsburg and L. D. Landau, Zh. Eksp. Teor. Fiz. 20, 1064 (1950). An English translation is included in *Men of Physics: L. D. Landau,* edited by D. ter Haar (Pergamon, New York, 1965), Vol. 1, p. 138.
[27]J. Bardeen, L. N. Cooper, and J. R. Schrieffer, Phys. Rev. 108, 1175 (1957).
[28]L. P. Gor'kov, Zh. Eksp. Teor. Fiz. 34, 735 (1958); [Sov. Phys. JETP 7, 505 (1958)]; 36, 1918 (1959) [9, 1364 (1959)].
[29]K. Maki, Physics (N.Y.) 1, 21 (1964); K. Maki, *ibid;* 1, 127 (1964); P. G. de Gennes, Phys. Kondens. Mater. 3, 79 (1964).
[30]E. Helfand and N. R. Werthamer, Phys. Rev. 147, 288 (1966).
[31]L. Neumann and L. Tewordt, Z. Phys. 189, 55 (1966); 191, 73 (1966).
[32]G. Eilenberger, Phys. Rev. 153, 584 (1967).
[33]U. Brandt, Phys. Lett. A 29, 568 (1969).
[34]J. M. Delrieu, J. Low Temp. Phys. 6, 197 (1972).
[35]E. H. Brandt, Phys. Status Solidi B 51, 345 (1972).
[36]W. Pesch and L. Kramer, J. Low Temp. Phys. 15, 367 (1974).
[37]E. H. Brandt, Phys. Status Solidi B 77, 105 (1976).
[38]P. C. Hohenberg and N. R. Werthamer, Phys. Rev. 153, 493 (1967).
[39]H. Teichler, Phys. Status Solidi B 69, 501 (1975); H. W. Pohl and H. Teichler, Phys. Status Solidi B 75, 205 (1976).
[40]K. Takanaka and A. Hubert, in *Proceedings of the Fourteenth International Conference on Low Temperature Physics, Otaniemi, Finland, 1975,* edited by M. Krusius and M. Vuorio (American Elsevier, New York, 1975), p. 309.
[41]K. Takanaka and T. Nagashima, Prog. Theor. Phys. (Kyoto) 43, 18 (1970).
[42]K. -H. Berthel and B. Pietrass, J. Low Temp. Phys. 33, 127 (1978).
[43]L. Leplae, H. Umezawa, and F. Mancini, Phys. Rep. C 10, 151 (1974).
[44]F. Mancini, M. Tachiki, and H. Umezawa, Physica (Utrecht) B 94, 1 (1978).
[45]J. B. Davidson and A. L. Case, in *Proceedings of the Conference on Neutron Scattering, Gatlinburg, Tennessee,* edited by R. Moon (ERDA CONF-760601-P2, Oak Ridge, Tennessee, 1976), p. 1124.
[46]S. T. Sekula and R. H. Kernohan, Phys. Rev. B 5, 904 (1972).
[47]The method is similar to that described by R. G. Chambers and J. G. Park, Brit. J. Appl. Phys. 12, 507 (1961). See also L. D. Landau and E. M. Lifshitz, *Electrodynamics of Continuous Media,* translated by J. B. Sykes and J. S. Bell (Pergamon, New York, 1960), p. 193.
[48]R. G. Younge (private communication); J. M. E. Harper, Ph. D. dissertation (Stanford University, 1975) (unpublished).
[49]J. L. Harden and V. Arp, Cryogenics 3, 105 (1963).
[50]F. C. von der Lage and H. A. Bethe, Phys. Rev. 71, 612 (1947).
[51]K. Fischer and H. Teichler, Phys. Lett. A 58, 402 (1976).

[52]B. B. Goodman, IBM J. Res. Dev. 6, 63 (1962).
[53]H. A. Leupold and H. A. Boorse, Phys. Rev. 134, A1322 (1964).
[54]C. Varmazis and M. Strongin, Phys. Rev. B 10, 1885 (1974).
[55]W. H. Butler (unpublished).
[56]L. F. Mattheiss, Phys. Rev. B 1, 373 (1970).
[57]P. J. Davis and P. Rabinowitz, *Methods of Numerical Integration* (Academic, New York, 1975), p. 365.
[58]F. B. Hildebrand, *Introduction to Numerical Analysis* (McGraw-Hill, New York, 1956), p. 314.